Article

The oldest tadpole reveals evolutionary stability of the anuran life cycle

https://doi.org/10.1038/s41586-024-08055-y

Received: 5 March 2024

Accepted: 16 September 2024

Published online: 30 October 2024

Check for updates

Mariana Chuliver[1]✉, Federico L. Agnolín[1,2], Agustín Scanferla[1,3], Mauro Aranciaga Rolando[2], Martín D. Ezcurra[4,5], Fernando E. Novas[2] & Xing Xu[6]

Anurans are characterized by a biphasic life cycle, with an aquatic larval (tadpole) stage followed by an adult (frog) stage, both connected through the metamorphic period in which drastic morphological and physiological changes occur[1]. Extant tadpoles exhibit great morphological diversity and ecological relevance[2], but their absence in the pre-Cretaceous fossil record (older than 145 million years) makes their origins and early evolution enigmatic. This contrasts with the postmetamorphic anuran fossil record that dates back to the Early Jurassic and with closely related species in the Late Triassic (around 217–213 million years ago (Ma))[3]. Here we report a late-stage tadpole of the stem-anuran *Notobatrachus degiustoi* from the Middle Jurassic of Patagonia (around 168–161 Ma). This finding has dual importance because it represents the oldest-known tadpole and, to our knowledge, the first stem-anuran larva. Its exquisite preservation, including soft tissues, shows features associated with the filter-feeding mechanism characteristic of extant tadpoles[4,5]. Notably, both *N. degiustoi* tadpole and adult reached a large size, demonstrating that tadpole gigantism occurred among stem-anurans. This new discovery reveals that a biphasic life cycle, with filter-feeding tadpoles inhabiting aquatic ephemeral environments, was already present in the early evolutionary history of stem-anurans and has remained stable for at least 161 million years.

Tadpoles are the free-living, non-reproductive aquatic larvae of anurans, which have to go through a metamorphic phase of profound morphological and ecological changes within a short period of time to reach the adult reproductive stage[1,2]. This drastic type of metamorphosis[6] of anurans is the most extreme among extant tetrapods, and tadpoles represent a highly derived larval stage[2,7]. Studies on the evolution of the tadpole morphospace indicated that key characters have evolved during the stem-anuran radiation around the Triassic–Jurassic boundary[8]. Nevertheless, these hypotheses are based solely on evidence from extant anurans and remain untested because fossil tadpoles are completely absent in the Triassic and Jurassic fossil record[9]. Moreover, stem-anurans are known only from postmetamorphic individuals[3,10–14]. Thus, the timing and evolutionary transformations involved in the origins of the tadpole body plan remain enigmatic and a matter of debate.

Here we describe the oldest-known tadpole from the Middle Jurassic La Matilde Formation (Bathonian–Callovian, around 168–161 million years ago (Ma)), based on a well-preserved specimen found in the Estancia La Matilde locality (Santa Cruz Province, Argentina), which is referred to the stem-anuran *Notobatrachus degiustoi*. This species is also represented by a large number of superbly preserved adult specimens from the same locality[13,15]. The exquisite preservation of the new specimen, including most of the hyobranchial apparatus and soft tissues, allows us to infer the mode of life and feeding habits of the *N. degiustoi* tadpole. Therefore, this finding substantially enhances our knowledge of the origins and early evolution of the biphasic anuran life cycle.

Description

The fossil MPM-PV (Museo Provincial Padre M.J. Molina, Río Gallegos, Santa Cruz Province, Argentina) 23540 is a single individual that consists of a cranium and most of the postcranium of a tadpole in dorsal aspect, including the proximal part of the tail (Fig. 1). It was collected from a quarry at Estancia La Matilde (the type locality of *N. degiustoi*)[15], where the La Matilde Formation crops out and which has also yielded hundreds of adult specimens of the species[13,15]. The finding of a single specimen is probably due to a collection bias related to taphonomic conditions, including autoecological traits and particular biostratinomic processes. Its occurrence in the same fossil levels as adults of *N. degiustoi*, the presence of several skeletal characteristics shared with adults of *N. degiustoi* (that is, nine presacral vertebrae, free ribs associated with presacrals II–IV, transverse processes of posterior presacral vertebrae as long as sacral diapophysis, uncinate process on free rib III), and the fact that no other anuran species have been

[1]Fundación de Historia Natural "Félix de Azara", Centro de Ciencias Naturales, Ambientales y Antropológicas, Universidad Maimónides, Ciudad Autónoma de Buenos Aires, Argentina. [2]Laboratorio de Anatomía Comparada y Evolución de los Vertebrados, CONICET–Museo Argentino de Ciencias Naturales "Bernardino Rivadavia", Ciudad Autónoma de Buenos Aires, Argentina. [3]Consejo Nacional de Investigaciones Científicas y Técnicas (CONICET), Ciudad Autónoma de Buenos Aires, Argentina. [4]Sección Paleontología de Vertebrados, CONICET–Museo Argentino de Ciencias Naturales "Bernardino Rivadavia", Ciudad Autónoma de Buenos Aires, Argentina. [5]School of Geography, Earth and Environmental Sciences, University of Birmingham, Edgbaston, Birmingham, UK. [6]Key Laboratory of Vertebrate Evolution and Human Origins, Institute of Vertebrate Paleontology and Paleoanthropology, Chinese Academy of Sciences, Beijing, China. ✉e-mail: marianachp@yahoo.com.ar

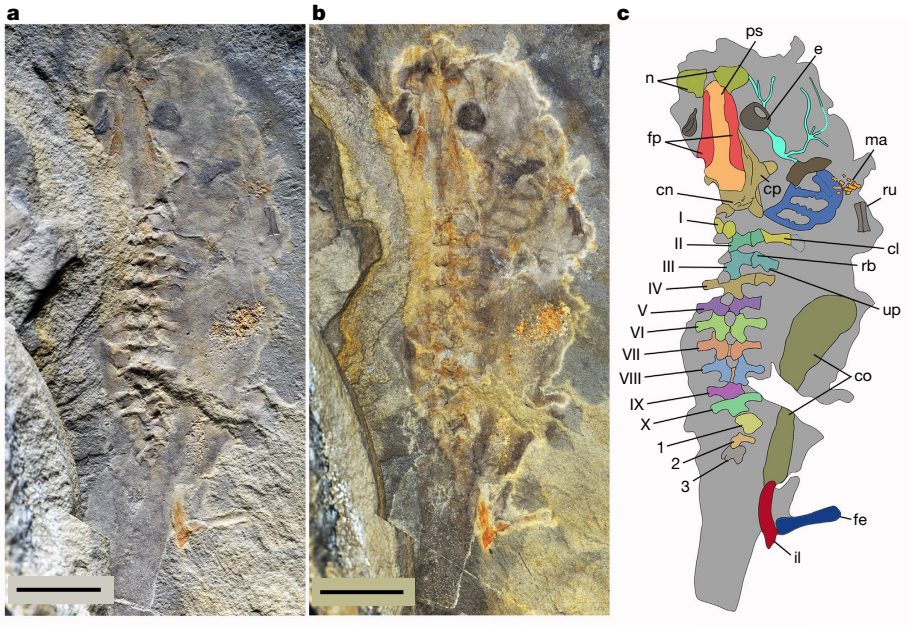

Fig. 1 | Photographs and interpretative drawing of specimen MPM-PV 23540. a, Photograph taken with short exposure time and low-angle white light enhancing the skeletal morphology. **b**, Photograph taken with long exposure time and high-angle white light enhancing soft tissue morphology. **c**, Interpretative drawing of the skeleton and soft tissues. cl, Cleithrum; cn, chondrified neurocranium; co, cololite; cp, crista parotica; e, eye; fe, femur; fp, frontoparietal; il, ilium; ma, manus; n, nasal; ps, parasphenoid; rb, rib; ru, radio-ulna; up, uncinate process; I–IX, presacral vertebrae; X, sacrum; 1–3, postsacral neural arches. Scale bars, 1 cm.

identified from the La Matilde Formation, support the referral of the fossil tadpole to this species. Geological data for the locality indicate that the sediments containing the specimen were deposited in the floodplain of a low-energy lentic environment, with pyroclastic input, under a seasonally dry–wet climate[16,17]. These sediments also contain diverse plants, branchiopod crustaceans, bivalves and insects (Extended Data Fig. 1)[18–20].

The tadpole was well chondrified, as indicated by cartilage imprints, and the overall degree of ossification supports an advanced larval stage before the beginning of metamorphosis (Extended Data Figs. 2–4). The cranial ossification that corresponds to the parasphenoid is flanked by the frontoparietals, which extend on both sides as longitudinal thin strips of bone, strongly tapering anteriorly and widely separated from each other along the midline (Fig. 1). The right otic region preserves the crista parotica, represented by a subtriangular, knob-like prominence (Fig. 1). The imprints of neural arches of nine presacral vertebrae, the sacrum and three postsacral vertebrae are present. The right forelimb is represented by the radius and ulna, fused to each other, and the manus (Fig. 1). The right iliac shaft is preserved in lateral view, with the dorsal acetabular expansion already ossified (Fig. 1). Based on the presence

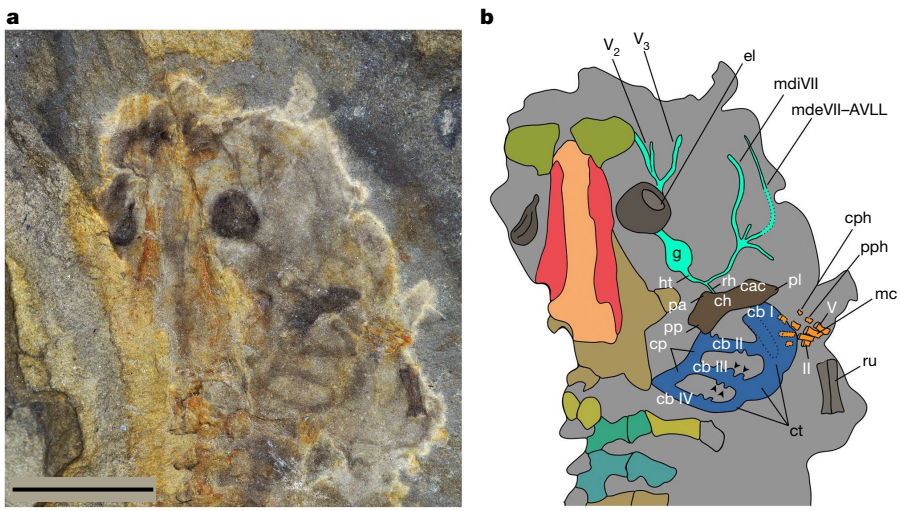

Fig. 2 | Photograph and interpretative drawing of the head region of specimen MPM-PV 23540. a, Photograph of the head region taken with long exposure time and high-angle white light, enhancing ossifications, hyobranchial skeleton and soft organs. **b**, Interpretative drawing depicting structures of the manus, hyobranchial skeleton and nerves. Medial and lateral projections of ceratobranchial III are indicated by arrowheads. cac, Condylus articularis of ceratohyal; cb, ceratobranchialia I–IV; ch, ceratohyal; cp, commissurae proximales; cph, central phalanx; ct, commissurae terminales; el, eye lens; g, ganglion; ht, hyomandibular trunk; mc, metacarpal; mdeVII–AVLL, ramus mandibularis externus of facial nerve and anteroventral lateral-line nerves; mdiVII, ramus mandibularis internus of facial nerve; pa, processus anterior; pl, processus lateralis; pp, processus posterior; pph, proximal phalanx; rh, ramus hyoideus; II, digit II; V, digit V; V_2, maxillary ramus of trigeminal nerve; V_3, mandibular ramus of trigeminal nerve. Scale bar, 1 cm.

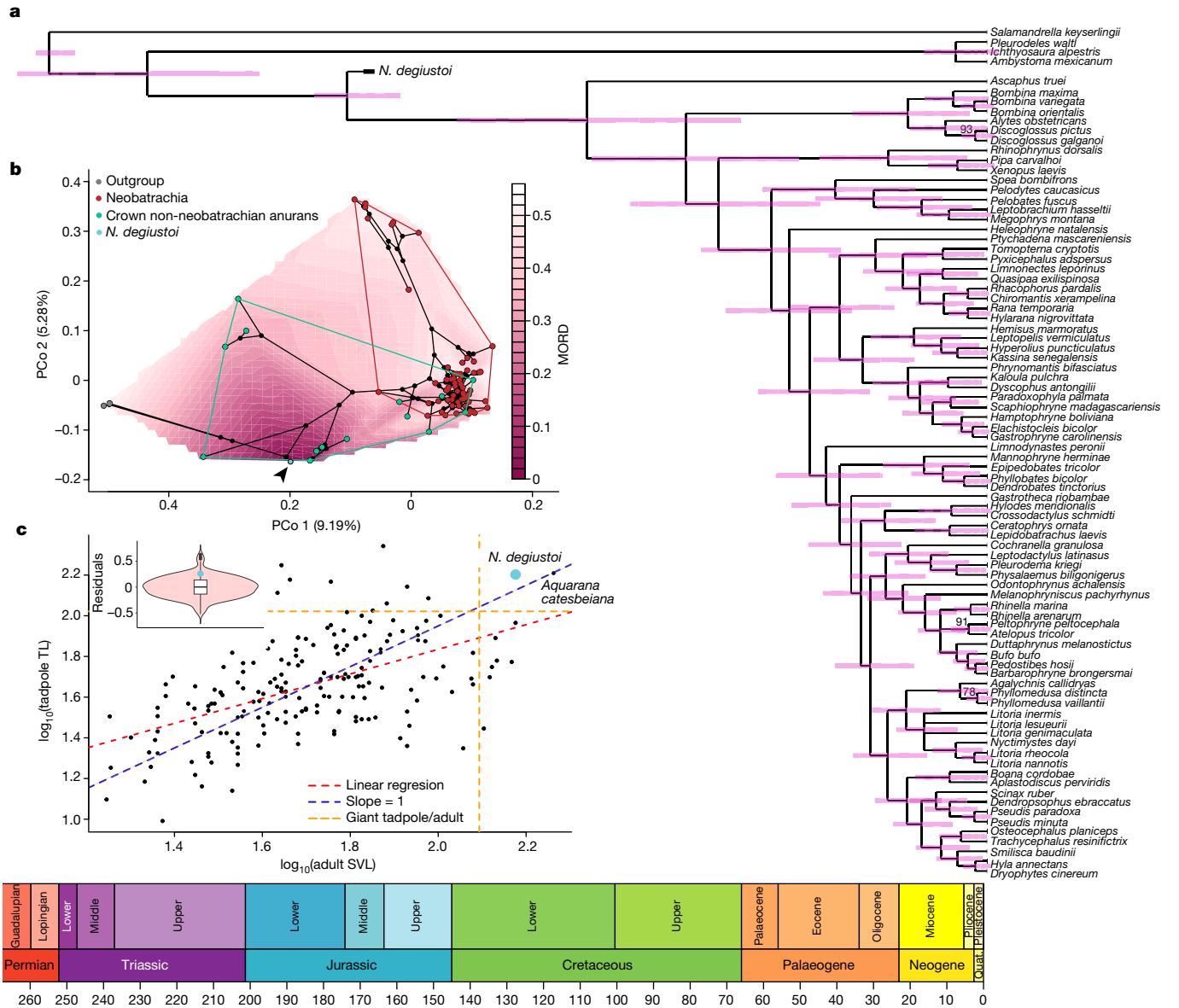

Fig. 3 | Phylogenetic affinities of the *N. degiustoi* tadpole. a, Time-calibrated Bayesian tip-dating tree based on tadpole anatomical characters and constrained following a molecular backbone of anuran phylogeny; violet bars indicate node temporal calibration, and numbers at nodes indicate posterior probabilities greater than 50% at non-topologically constrained nodes. **b**, Phylomorphospace of the first two principal coordinates and dissimilarity distances (MORD) as a heatmap, showing the *N. degiustoi* tadpole (light blue dot indicated by arrowhead) close to crown non-neobatrachian tadpoles (green dots). **c**, Bivariate plot of $\log_{10}$-transformed tadpole total length (TL) versus $\log_{10}$-transformed adult snout–vent length (SVL) (residuals shown as a violin plot at top left; $n = 190$ species; median 0.0027; lower and whiskers −0.5212–0.5469; box limits −0.1364–0.1377). Dashed red line represents linear generalized least-squares regression ($R^2 = 0.2855$, $P < 0.001$); dashed blue line represents slope = 1; top right quadrate delimited by orange dashed lines indicates the area occupied by species with both giant tadpoles and adults—that is, *N. degiustoi* and the extant American bullfrog *Aquarana catesbeiana*. PCo, principal coordinates; quat., Quaternary.

of the forelimb still contained within the body contour, probably covered by the operculum, and the stage of development of cranial and postcranial ossifications[21–23] (detailed in Supplementary Information), we assign the tadpole to Gosner stages 40–41 (ref. 24).

MPM-PV 23540 is unique in regard to preservation of the hyobranchial skeleton, which was not preserved in any other fossil tadpole described to date[9]. The expanded ceratohyal possesses well-developed anterior, posterior and lateral processes and a condylus articularis (Fig. 2), indicating the presence of an articulation with the palatoquadrate cartilage. Ceratobranchialia are preserved as four dark, mediolaterally oriented bands with ellipsoidal fields between them, representing branchial slits (Fig. 2). Ceratobranchial I is medially overlapped by the ceratohyal. Ceratobranchials II–IV are proximally connected by commissurae proximales, and distally by commissurae terminales (Fig. 2). Medial and lateral projections for support of the gill filters are distinguished along the shafts of ceratobranchialia II and III. An oblique, rod-like element is positioned lateroventral to the ceratohyal and lateral to ceratobranchial I (Fig. 2); it could represent the lateral projection of the hypobranchial plate, although its identity is doubtful.

Soft parts, including eyes and nerves, are preserved as dark imprints in their anatomical position. The eyes are dorsally positioned; the lens within the right eye is clearly distinguishable on the anterolateral region of the eyeball, which is indicative of an anterolaterally facing eye (Fig. 2). Several nerve impressions are distinguishable on the right side of the cranial region (Fig. 2 and Supplementary Information).

Analyses and discussion

We explored the phylogenetic relationships of the *N. degiustoi* tadpole using a modified phylogenetic dataset based on tadpole traits[8]. This new dataset comprises 86 species scored for 152 characters (Supplementary information). The tadpole of *N. degiustoi* was recovered as a stem-Anura using both implied weighted-maximum parsimony and Bayesian inference with a relaxed Markov *k*-state variable morphological clock model that incorporates taxon ages using a fossilized birth–death process (Fig. 3a). These results are consistent with those previously found based exclusively on the adult morphology of *N. degiustoi*[12,25,26]. Despite the adaptive decoupling between larva and adult in anurans[27,28], the morphology of both semaphoronts (that is, tadpole and adult) has congruent phylogenetic signals and retrieves consistent phylogenetic positions for both crown and stem-anurans.

Several anatomical traits present in the *N. degiustoi* tadpole demonstrate that key features of crown-anuran tadpoles had already evolved in stem taxa—in particular, the structures of the hyobranchial skeleton involved in the feeding mechanism. The filter-feeding system of the vast majority of extant tadpoles consists of a complex buccopharyngeal filter apparatus that entraps food particles from water currents, maintained by the continuous action of a buccal pump[4,29]. Commissurae terminales, commissurae proximales, a ceratohyale with a median horizontal plate lacking a distinct processus anterolateralis, and spiny projections on ceratobranchials are traits of the hyobranchial skeleton of extant tadpoles closely related to the filter-feeding mechanism[7,30,31], which were already present in the *N. degiustoi* tadpole. Moreover, the phylomorphospace built based on the dataset of tadpole features also shows that *N. degiustoi* is positioned close in the morphospace to early-diverging crown-anuran tadpoles, and has the lowest dissimilarity distance with respect to them (Fig. 3b). In other words, the general morphology described here for the tadpole of the stem-anuran *N. degiustoi* is highly congruent with that of extant anurans such as discoglossoids.

Giant tadpoles are defined here as those having a total length equal to or higher than twice the mean of the total length of the species sampled in our dataset (over 101.8 mm; Extended Data Fig. 9). Thus, the estimated total length of 159 mm for the *N. degiustoi* tadpole is above the threshold of gigantism (Supplementary Information), approaching that of normal giant tadpoles of extant frog species such as the paradoxical frog *Pseudis paradoxa*, whose giant tadpoles occur naturally and successfully metamorphose[32,33]. The developmental stage of the *N. degiustoi* tadpole (Gosner stage 40–41) indicates that it was close to reaching the metamorphic phase, thus allowing us to discard a pathological (for example, athyroid) condition to explain gigantism in this specimen.

Notably, adults of *N. degiustoi*—by far the largest stem-anuran and one of the largest Mesozoic anurans (Supplementary Table 1)—reached a body size of 150 mm (ref. 13), falling within the range of giant adult anurans (over 127 mm of snout–vent length)[34]. Gigantism in tadpoles and postmetamorphic anurans has evolved several times in the history of the clade[34,35], but there are few species for which both tadpoles and postmetamorphic individuals are giants (Fig. 3c and Supplementary Table 2). Phylogenetic optimization of the residuals of a regression between tadpole total length and adult snout–vent length indicates that larval gigantism in *N. degiustoi* evolved independently from gigantism in crown anurans (Extended Data Fig. 9). Under regular conditions, there are two ways in which a normal tadpole might become gigantic, namely a long development (predisplacement or hypermorphosis) or accelerated developmental rates[36]. This depends on ecological factors such as environmental stability (food availability, low risk of desiccation) and the absence of predators[7,37]. According to fossil data of the locality, interspecific competence and predator pressures were negligible. Therefore, the large size of the *N. degiustoi* tadpole could be the result of both factors, an increase in developmental time and growth in seasonally ephemeral ponds.

The palaeoecology of the locality and the anatomical information provided here indicate that an exotrophic filter-feeding tadpole inhabiting lentic ephemeral microhabitats is the ancestral condition for anurans, in agreement with previous studies based on extant species[31,38–40]. Therefore, the overall morphology of *N. degiustoi* indicates that the anuran biphasic life cycle with marked metamorphosis was already present 161 Ma in the Middle Jurassic. These findings are consistent with studies of the larval body plan of living anurans, suggesting that tadpole morphological novelties, such as those associated with filter-feeding mechanisms, evolved in a radiation around the Triassic–Jurassic boundary[8]. The marked anatomical similarity between the *N. degiustoi* tadpole and extant early-diverging crown-anuran tadpoles further supports this evolutionary scenario, which was probably promoted by the stable selective pressures of ephemeral freshwater habitats exploited by anurans since the early phases of their evolutionary history.

Online content

Any methods, additional references, Nature Portfolio reporting summaries, source data, extended data, supplementary information, acknowledgements, peer review information; details of author contributions and competing interests; and statements of data and code availability are available at https://doi.org/10.1038/s41586-024-08055-y.

1. Handrigan, G. R. & Wassersug, R. J. The anuran Bauplan: a review of the adaptive, developmental, and genetic underpinnings of frog and tadpole morphology. *Biol. Rev.* **82**, 1–25 (2007).
2. McDiarmid, R. W. & Altig, R. *Tadpoles: the Biology of Anuran Larvae* (Univ. of Chicago Press, 1999).
3. Stocker, M. R. et al. The earliest equatorial record of frogs from the Late Triassic of Arizona. *Biol. Lett.* **15**, 20180922 (2019).
4. Kenny, J. S. Feeding mechanisms in anuran larvae. *J. Zool. (1987)* **157**, 225–246 (1969).
5. Wassersug, R. J. & Hoff, K. A comparative study of the buccal pumping mechanism of tadpoles. *Biol. J. Linn. Soc.* **12**, 225–259 (1979).
6. Schoch, R. R. & Witzmann, F. The evolution of larvae in temnospondyls and the stepwise origin of amphibian metamorphosis. *Biol. Rev.* https://doi.org/10.1111/brv.13084 (2024).
7. Wassersug, R. J. The adaptive significance of the tadpole stage with comments on the maintenance of complex life cycles in anurans. *Amer. Zool.* **15**, 405–417 (1975).
8. Roelants, K., Haas, A. & Bossuyt, F. Anuran radiations and the evolution of tadpole morphospace. *Proc. Natl Acad. Sci. USA* **108**, 8731–8736 (2011).
9. Gardner, J. D. The fossil record of tadpoles. *Fossil Imprint* **72**, 17–44 (2016).
10. Reig, O. A. Noticia sobre un nuevo anuro fósil del Jurásico de Santa Cruz (Patagonia). *Ameghiniana* **2**, 73–78 (1961).
11. Shubin, N. H. & Jenkins, F. A. An Early Jurassic jumping frog. *Nature* **377**, 49–52 (1995).
12. Báez, A. M. & Basso, N. G. The earliest known frogs of the Jurassic of South America: review and cladistic appraisal of their relationship. *Münchner Geowiss. Abh. (A)* **30**, 131–158 (1996).
13. Báez, A. M. & Nicoli, L. A new look at an old frog: the Jurassic *Notobatrachus* Reig from Patagonia. *Ameghiniana* **41**, 257–270 (2004).
14. Gao, K. Q. & Chen, S. A new frog (Amphibia: Anura) from the Lower Cretaceous of western Liaoning, China. *Cretac. Res.* **25**, 761–769 (2004).
15. Stipanicic, P. N. & Reig, O. A. El "Complejo porfírico de la Patagonia extraandina" y su fauna de anuros. *Acta Geol. Lilloana* **1**, 185–298 (1957).
16. De Barrio, R. E., Panza, J. L. & Nullo, F. E. in *Geología Argentina* (ed. Caminos, R.) 511–527 (Instituto de Geología y Recursos Minerales, 1999).
17. Rees, P. M. et al. in *Warm Climates in Earth History* (eds Huber, B. T. et al.) 297–318 (Cambridge Univ. Press, 2000).
18. Gallego, O. F. Conchóstracos (Cyzicidae) del Jurásico de Santa Cruz y Chubut, Argentina. *Ameghiniana* **30**, 333–345 (1994).
19. Zamuner, A. B. & Falaschi, P. *Agathoxylon matildense* n. sp., leño araucariaceo del Bosque Petrificado del cerro Madre e Hija, Formación La Matilde (Jurásico medio), provincia de Santa Cruz, Argentina. *Ameghiniana* **42**, 339–346 (2005).
20. Gnaedinger, S. Podocarpaceae woods (Coniferales) from Middle Jurassic La Matilde formation, Santa Cruz Province, Argentina. *Rev. Palaeobot. Palyno.* **147**, 77–93 (2007).
21. Trueb, L. in *The Skull, Vol. 2. Patterns of Structural and Systematic Diversity* (eds Hanken, J. & Hall, B. K.) 255–343 (Univ. of Chicago Press, 1993).
22. Ročková, H. & Roček, Z. Development of the pelvis and posterior part of the vertebral column in the Anura. *J. Anat.* **206**, 17–35 (2005).
23. Havelková, P. & Roček, Z. Transformation of the pectoral girdle in the evolutionary origin of frogs: insights from the primitive anuran *Discoglossus*. *J. Anat.* **209**, 1–11 (2006).
24. Gosner, K. L. A simplified table for staging anuran embryos and larvae with notes on identification. *Herpetologica* **16**, 183–190 (1960).
25. Gao, K.-Q. & Wang, Y. Mesozoic anurans from Liaoning Province, China, and phylogenetic relationships of archaeobatrachian anuran clades. *J. Vertebr. Paleontol.* **21**, 460–476 (2001).

26. Marjanović, D. & Laurin, M. An updated paleontological timetree of lissamphibians, with comments on the anatomy of Jurassic crown-group salamanders (Urodela). *Hist. Biol.* **26**, 535–550 (2014).
27. Sherratt, E., Vidal-García, M., Anstis, M. & Keogh, J. S. Adult frogs and tadpoles have different macroevolutionary patterns across the Australian continent. *Nat. Ecol. Evol.* **1**, 1385–1391 (2017).
28. Wollenberg Valero, K. et al. Transcriptomic and macroevolutionary evidence for phenotypic uncoupling between frog life history phases. *Nat. Commun.* **8**, 15213 (2017).
29. Wassersug, R. J. The mechanism of ultraplanktonic entrapment in anuran larvae. *J. Morphol.* **137**, 279–288 (1972).
30. Haas, A. The larval hyobranchial apparatus of discoglossoid frogs: its structure and bearing on the systematics of the Anura (Amphibia: Anura). *J. Zool. Syst. Evol. Res.* **35**, 179–197 (1997).
31. Cannatella, D. in *Tadpoles: the Biology of Anuran Larvae* (eds McDiarmid, R. W. & Altig, R.) 52–91 (Univ. of Chicago Press, 1999).
32. Emerson, S. The giant tadpole of *Pseudis paradoxa*. *Biol. J. Linn. Soc.* **34**, 93–104 (1988).
33. Fabrezi, M., Quinzio, S. I. & Goldberg, J. The giant tadpole and delayed metamorphosis of *Pseudis platensis* Gallardo, 1961 (Anura: Hylidae). *J. Herpetol.* **43**, 228–243 (2009).
34. Womack, M. C. & Bell, R. C. Two-hundred million years of anuran body-size evolution in relation to geography, ecology and life history. *J. Evolution. Biol.* **33**, 1417–1432 (2020).
35. Roček, Z., Böttcher, R. & Wassersug, R. J. Gigantism in the tadpoles of the Neogene frog *Paleobatrachus*. *Paleobiology* **32**, 666–675 (2006).
36. Fabrezi, M. Heterochrony in growth and development in anurans from the Chaco of South America. *Evol. Biol.* **38**, 390–411 (2011).
37. Skelly, D. K. Tadpole communities. *Am. Sci.* **85**, 36–45 (1997).
38. Orton, G. L. The systematics of vertebrate larvae. *Syst. Zool.* **2**, 63–75 (1953).
39. Duellman, W. E. & Trueb, L. *Biology of Amphibians* (McGraw-Hill, 1986).
40. Hanken, J. in *The Origin and Evolution of Larval Forms* (eds Hall, B. K. & Wake, M. H.) 61–108 (Academic, 1999).

Methods

Morphological description

Osteological terminology follows Trueb[21,41] and Pugener and Maglia[42]. Vertebrae are designated using Roman numerals in anteroposterior order. Vertebra X is referred to as the sacrum. Postsacral vertebrae are designated in an anterior-to-posterior sequence using Arabic numerals. Structures of the suspension filter-feeding system are referred according to Wassersug[43]. Terms for hyobranchial skeleton follow Haas[30], with nervous system structures following the terminology of Schlosser and Roth[44].

Phylogenetic analyses

The phylogenetic position of the *N. degiustoi* tadpole was tested using a phylogenetic data matrix including 86 taxa and 152 characters, modified from the analysis of Haas[45]. A Bayesian tip-dating analysis was conducted in MrBayes 3.2.7a[46]. We used an Mkv substitution model, the same list of ordered characters as in Roelants et al.[8] and *Salamandrella keyserlingii* as the outgroup. We used an independent gamma-rate, relaxed-clock model and uniform age priors modelled around the first and last appearance dates for all tips of the tree. We implemented a node age calibration for Discoglossidae (uniform prior of 120.0–120.1 Ma (ref. 47)), Pipoidea (uniform prior of 113.0–113.1 Ma (ref. 48)), Anomocoela (uniform prior of 52.0–52.1 Ma (ref. 49) and Pyxicephalidae (uniform prior of 39.5–39.6 Ma (ref. 50)). We specified a fossilized birth–death process as the tree model using standard parameterizations and values. Fossils were specified to be tips and that the fraction of extant species represented 98.8% of the terminals. The deepest split within the tree was parameterized with a uniform tree age prior of 250.0–272.8 Ma, following the minimum and soft maximum ages of Benton et al.[51] for crown-Batrachia. We used metropolis coupling Markov chain Monte Carlo algorithms with two independent runs of 24 chains, using a heating coefficient of 0.05 and three swap attempts per generation. Topological convergence, as indicated by average standard deviation of split frequencies decreasing below 0.01, was achieved following 15,435,000 generations (Extended Data Fig. 5). A potential scale reduction factor of 1.0, visual inspection of trace plot with Tracer 1.7.1 (ref. 52) and estimated sample sizes for all parameters over 200 further indicated convergence. A second analysis was performed with the same settings, except that the topology was constrained following a molecular backbone of anuran phylogeny (Extended Data Fig. 6) based on the results of Jetz and Pyron[53]. This analysis reached average standard deviation of split frequencies below 0.001 following 4,010,000 generations.

The data matrix was also analysed under implied weighted-maximum parsimony with a range of concavity constant values (*k*) between 7 and 10 (ref. 54) and using the program TNT 1.6 (ref. 55). It used the same list of ordered characters as in the Bayesian inference analysis. The search strategies started with the calculation of Wagner trees and using a combination of the tree-search algorithms tree bisection and reconnection branch swapping, sectorial searches, ratchet and tree fusing, until 100 hits of the same minimum tree length were achieved. The best trees obtained were subjected to a final round of tree bisection and reconnection branch swapping. Zero-length branches in any of the recovered most parsimonious trees were collapsed, and all trees were rooted with *S. keyserlingii*. A global strict consensus tree was generated from the most parsimonious trees found in the analyses using different *k* values (Extended Data Fig. 7). Homoplasy indices for each analysis under the different *k* values were calculated with a script that does not consider a priori deactivated terminals ('STATSb.run'). Group supports were quantified using no-zero weight symmetric resampling analyses, with 10,000 technical pseudoreplications and reporting both absolute and group present/contradicted frequencies. Resampling frequencies were calculated from all resampling trees recovered using the different *k* values and plotted on the branches of the global strict consensus tree.

A further analysis was conducted following the same matrix settings, tree-search strategy, homoplasy index calculation and resampling analyses as before, but using a topological constrain based on the molecular backbone of anuran phylogeny (Extended Data Fig. 8) that follows the results of Jetz and Pyron[53]. These parsimony analyses were implemented in two custom scripts written here for TNT ('treeSearches_protocol_Notobatrachus_constrained.run' and 'treeSearches_protocol_Notobatrachus_unconstrained.run').

Morphological disparity analysis

Tadpole morphological diversity (disparity) was quantified on the taxon–character matrix modified from Roelants et al.[8] using the R package Claddis v.0.6.3 (ref. 56). This matrix is the same as that used for the phylogenetic analyses (86 species versus 152 discrete morphological characters). The distance matrix was generated from the taxon–character matrix with MORD[56], because the commonly used generalized Euclidean distance may produce a strong methodological bias in matrices with a moderate to high amount of missing data[57–59]. An ordination of the distance matrix was performed using a PCo analysis with Lingoes correction because of the presence of negative eigenvalues. No species had to be trimmed to conduct the ordination because no data were missing in the distance matrix. The phylomorphospace was plotted using the first two principal coordinates, which account for 14.47% of the total variance of the dataset, and the majority rule consensus tree with mean ages of the time-calibrated Bayesian inference analysis. Ancestral node estimations and their position in the morphospace were conducted with the 'phylomorphospace' function of the R package phytools v.2.1-1 (ref. 60). Extant anurans were graphically differentiated between non-neobatrachians and neobatrachians. Finally, a heatmap depicting the MORD of each species to *N. degiustoi* was superimposed onto the phylomorphospace biplot to show the raw distance between tadpole morphologies and their evolutionary divergence through time. The heatmap was built with the function 'filled.contour' of the R package akima v.0.6-3.4 (ref. 61).

Morphometric analyses

We performed an exhaustive literature search for descriptions with measurements of tadpoles and adults of extant and extinct anuran species (Supplementary Table 2). For each species, we recorded tadpole body length and maximum total length, and adult maximum snout–vent length. To reflect the size just before metamorphosis, we used measurements only from individuals at Gosner stages 39–41, approximately the range to which the *N. degiustoi* tadpole is assigned. For adults, we took the largest measurement found in the literature. Our sampling includes 35 of 50 anuran families and a total of 187 species. This information is detailed, along with literature resources, in Supplementary Table 2.

For estimatation of the total length of the *N. degiustoi* tadpole, we built a linear regression model of body length against total length. Data on tadpole body length were available for fewer species than those for total length, and therefore we had to reduce our dataset (Supplementary Table 3). A Shapiro–Wilk test was first performed to address whether each trait was normally distributed under the null hypothesis that the distribution was normal.

Because we found no agreement for the definition of a gigantic tadpole, we defined it as those specimens having a total length equal to or higher than twice the mean of the total length of the species sampled in our dataset. According to our database, the average total length among sampled specimens was 50.94 mm ($n = 190$; s.d. = ±28.2); therefore, those tadpoles with a total length equal to or above 101.8 mm were classified as giants (Extended Data Fig. 9). Afterwards, to determine whether tadpole and adult body sizes were significantly related and, in consequence, whether giant tadpoles were related to giant adults, we tested the relationship between tadpole and adult body size among species. We followed Womack and Bell[34] for the description

of giant adults, defined as those having snout–vent length greater than 127 mm. We plotted log-transformed tadpole total length versus log-transformed adult snout–vent length, and calculated a linear generalized least-squares regression between these variables. We have not conducted a phylogenetic generalized least squares because available phylogenetic trees and our dataset of measurements do not share most of the species-level taxa and, to include phylogeny in the variance of the regression, we would have had to prune most of the data. A violin plot of the residuals of this regression was plotted, and we highlighted the position of the residual of *N. degiustoi*. The residuals have been also optimized in the Bayesian inference tree following pruning of species not included in the regression analysis and using maximum likelihood as the optimality criterion ('contMap' function of the R package phytools v.2.1-1 (ref. 60)). All graphics and regression were conducted in R 4.2.3 (ref. 62).

Reporting summary

Further information on research design is available in the Nature Portfolio Reporting Summary linked to this article.

Data availability

All data generated or analysed during the study are included as part of this Article and its Supplementary Information files. The datasets for phylogenetic, disparity and morphometric analyses are available at Figshare (https://doi.org/10.6084/m9.figshare.25339195)[63].

Code availability

The data matrix used for phylogenetic analyses is available at Figshare (https://figshare.com/s/4fc207d07da2b8ff13cd?file=44846395)[64] and can be accessed from the project entitled '*Notobatrachus* tadpole'. The R codes used for phylogenetic, disparity and morphometric analyses are also available at Figshare (https://doi.org/10.6084/m9.figshare.25339195)[63].

41. Trueb, L. in *Evolutionary Biology of the Anurans, Contemporary Research on Major Problems* (ed. Vial, J. L.) 65–132 (Univ. of Missouri Press, 1973).
42. Pugener, L. A. & Maglia, A. M. Developmental evolution of the anuran sacro-urostylic complex. *S. Am. J. Herpetol.* **4**, 193–209 (2009).
43. Wassersug, R. J. Oral morphology of anuran larvae: terminology and general description. *Occas. Pap. Mus. Nat. Hist. Univ. Kansas* **48**, 1–23 (1976).
44. Schlosser, G. & Roth, G. Distribution of cranial and rostral spinal nerves in tadpoles of the frog *Discoglossus pictus* (Discoglossidae). *J. Morphol.* **226**, 189–212 (1995).
45. Haas, A. Phylogeny of frogs as inferred from primarily larval characters (Amphibia: Anura). *Cladistics* **19**, 23–89 (2003).
46. Ronquist, F. et al. MrBayes 3.2: efficient Bayesian phylogenetic inference and model choice across a large model space. *Syst. Biol.* **61**, 539–542 (2012).
47. Báez, A. M. Anurans from the Early Cretaceous Lagerstätte of Las Hoyas, Spain: new evidence on the Mesozoic diversification of crown-clade Anura. *Cretac. Res.* **41**, 90–106 (2013).
48. Carvalho, I. S. et al. A new genus of pipimorph frog (Anura) from the early Cretaceous Crato formation (Aptian) and the evolution of South American tongueless frogs. *J. S. Am. Earth Sci.* **92**, 222–233 (2019).
49. Henrici, A. C., Báez, A. M. & Grande, L. *Aerugoamnis paulus*, new genus and new species (Anura: Anomocoela): first reported Anuran from the Early Eocene (Wasatchian) fossil Butte member of the Green River formation, Wyoming. *Ann. Carnegie Mus.* **81**, 295–309 (2013).
50. Lemierre, A., Folie, A., Bailon, S., Robin, N. & Laurin, M. From toad to frog, a CT-based reconsideration of *Bufo servatus*, an Eocene anuran mummy from Quercy (France). *J. Vertebr. Paleontol.* https://hal.science/hal-03501090 (2021).
51. Benton, M. J. et al. Constraints on the timescale of animal evolutionary history. *Palaeontol. Electron.* **18.1.1FC**, 1–106 (2015).
52. Rambaut, A., Drummond, A. J., Xie, D., Baele, G. & Suchard, M. A. Posterior summarization in Bayesian phylogenetics using Tracer 1.7. *Syst. Biol.* **67**, 901–904 (2018).
53. Jetz, W. & Pyron, R. A. The interplay of past diversification and evolutionary isolation with present imperilment across the amphibian tree of life. *Nat. Ecol. Evol.* **21**, 850–858 (2018).
54. Ezcurra, M. D. Exploring the effects of weighting against homoplasy in genealogies of palaeontological phylogenetic matrices. *Cladistics* **40**, 242–281 (2024).
55. Goloboff, P. & Morales, M. TNT version 1.6, with a graphical interface for MacOs and Linux, including new routines in parallel. *Cladistics* **39**, 144–153 (2023).
56. Lloyd, G. T. Estimating morphological diversity and tempo with discrete character-taxon matrices: implementation, challenges, progress, and future directions. *Biol. J. Linn. Soc.* **118**, 131–151 (2016).
57. Ezcurra, M. D. & Butler, R. J. The rise of the ruling reptiles and ecosystem recovery from the Permo-Triassic mass extinction. *Proc. R. Soc. B Biol. Sci.* **285**, 20180361 (2018).
58. Flannery Sutherland, J. T., Moon, B. C., Stubbs, T. L. & Benton, M. J. Does exceptional preservation distort our view of disparity in the fossil record? *Proc. Biol. Sci.* **286**, 20190091 (2019).
59. Lehmann, O. E., Ezcurra, M. D., Butler, R. J. & Lloyd, G. T. Biases with the Generalized Euclidean Distance measure in disparity analyses with high levels of missing data. *Palaeontology* **62**, 837–849 (2019).
60. Revell, L. J. Phytools: an R package for phylogenetic comparative biology (and other things). *Methods Ecol. Evol.* **3**, 217–223 (2012).
61. Akima, H., Gebhardt, A., Petzold, T. & Maechler, M. akima: Interpolation of irregularly and regularly spaced data. https://cran.r-project.org/web/packages/akima/index.html (2021).
62. R Core Team. *R: A Language and Environment for Statistical Computing* (R Foundation for Statistical Computing, 2023).
63. Chuliver, M. Datasets used for phylogenetic analyses of the manuscript entitled 'The oldest tadpole reveals evolutionary stability of the anuran life cycle'. Figshare https://doi.org/10.6084/m9.figshare.25339195.v1 (2024).
64. Chuliver, M. Data matrix used for phylogenetic analyses of the manuscript entitled 'The oldest tadpole reveals evolutionary stability of the anuran life cycle'. Figshare https://figshare.com/s/4fc207d07da2b8ff13cd (2024).

Acknowledgements This study was supported by Agencia Nacional de Promoción Científica y Técnica (no. PICT 2020-02443) to A.S., and by the National Natural Science Foundation of China (grant No. 42288201) and Yunnan Revitalization Talent Support Program (no. 202305AB350006) to X.X. We also thank N. Vega (LAHN – CNEA) for microcomputed tomography facilities, V. D'Acurso (CITEDEF) for technical assistance, A. Haas (LIB) for providing files of phylogenetic matrices, and M. Isasi (MACN – CONICET) for technical preparation of the fossil specimen. We thank A. Di Federico and M. A. Queizán (Advanced Machine Systems) for 3D scanning, high-resolution tomography (Zeiss Metrotom), and post-processing of images. This study used computational resources from Universidad Nacional de Córdoba (https://ccad.unc.edu.ar/), which are part of SNCAD – MinCyT, Argentina. We also thank the Willi Hennig Society for supporting the free use of TNT software. Special thanks go to the team that excavated at the Estancia La Matilde locality in 2018.

Author contributions M.C., F.L.A. and A.S. contributed equally to project conceptualization, analysis and writing of the original draft. M.C. and A.S. scored phylogenetic matrices, gathered analytic data and performed statistical analyses. M.A.R. conducted specimen curation and created the figures with input from M.C. and A.S. M.D.E. conducted methodological development and phylogenetic and morphological disparity analyses and their visualization. F.L.A., F.E.N. and X.X. contributed material, field trip logistics and funding acquisition. All authors contributed to writing the manuscript, discussion and conclusions.

Competing interests The authors declare no competing interests.

Additional information

Supplementary information The online version contains supplementary material available at https://doi.org/10.1038/s41586-024-08055-y.

Correspondence and requests for materials should be addressed to Mariana Chuliver.

Peer review information *Nature* thanks Liping Dong, Nadia Fröbisch, James Gardner and Zbyněk Roček for their contribution to the peer review of this work. Peer reviewer reports are available.

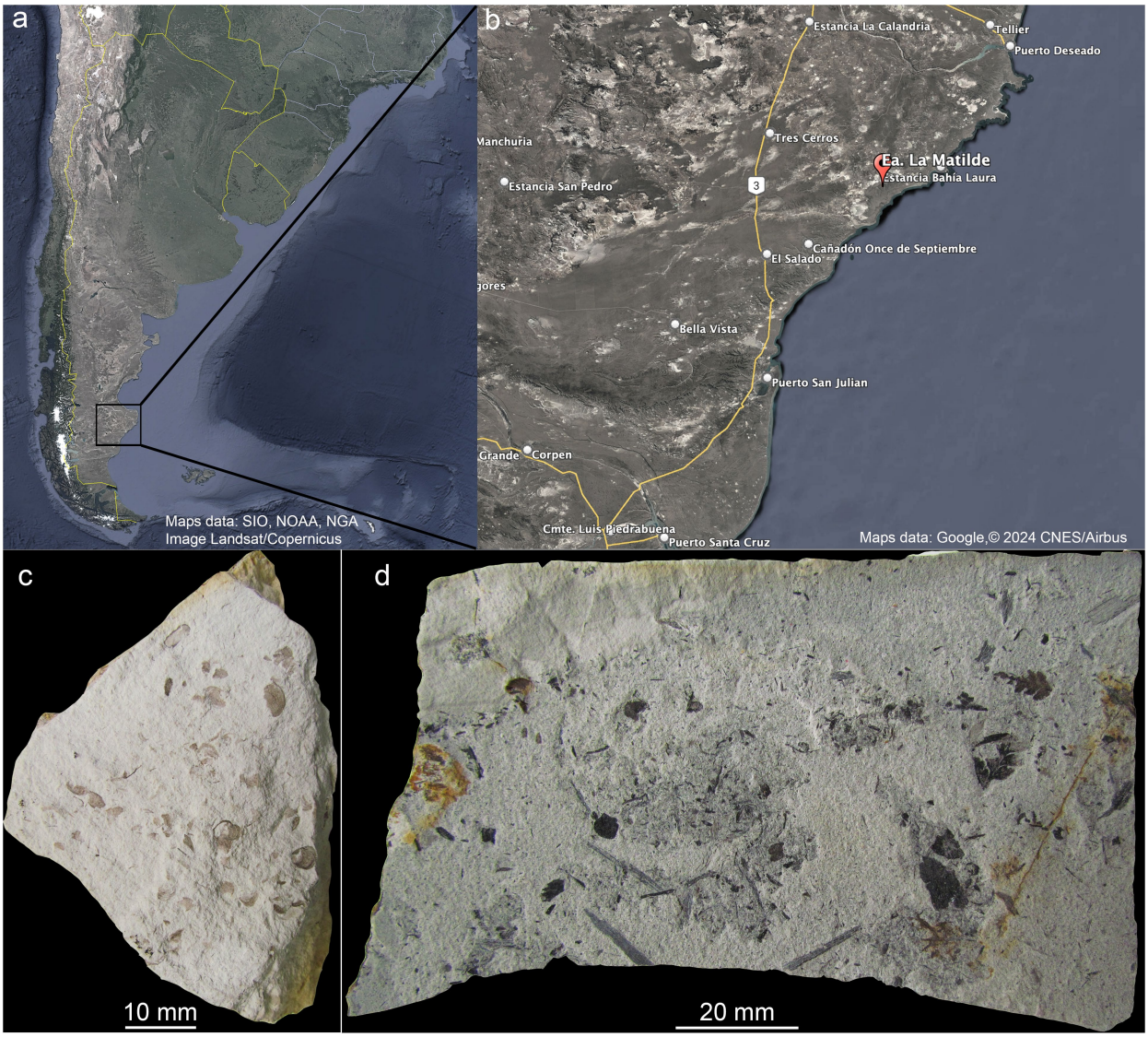

Extended Data Fig. 1 | Geographic location and fossils found at the La Matilde locality. a,**b**, Geographic location of the Estancia La Matilde locality (type locality of *Notobatrachus degiustoi*), in Santa Cruz Province, Argentina. **c**,**d**, Several specimens of the branchiopod *Eosolimnadiopsis? santacrucensis* and plant debris frequently found in the same levels as *N. degiustoi* specimens in the Estancia La Matilde locality. Abbreviations: Ea, Estancia.

Extended Data Fig. 2 | Specimen in high resolution. High-resolution photograph of MPM-PV 23540 taken under long exposure time and sub-vertical artificial white light.

Extended Data Fig. 3 | Specimen in high resolution. High-resolution photograph of MPM-PV 23540 taken under short exposure time and low-angle artificial white light coming from the upper left corner.

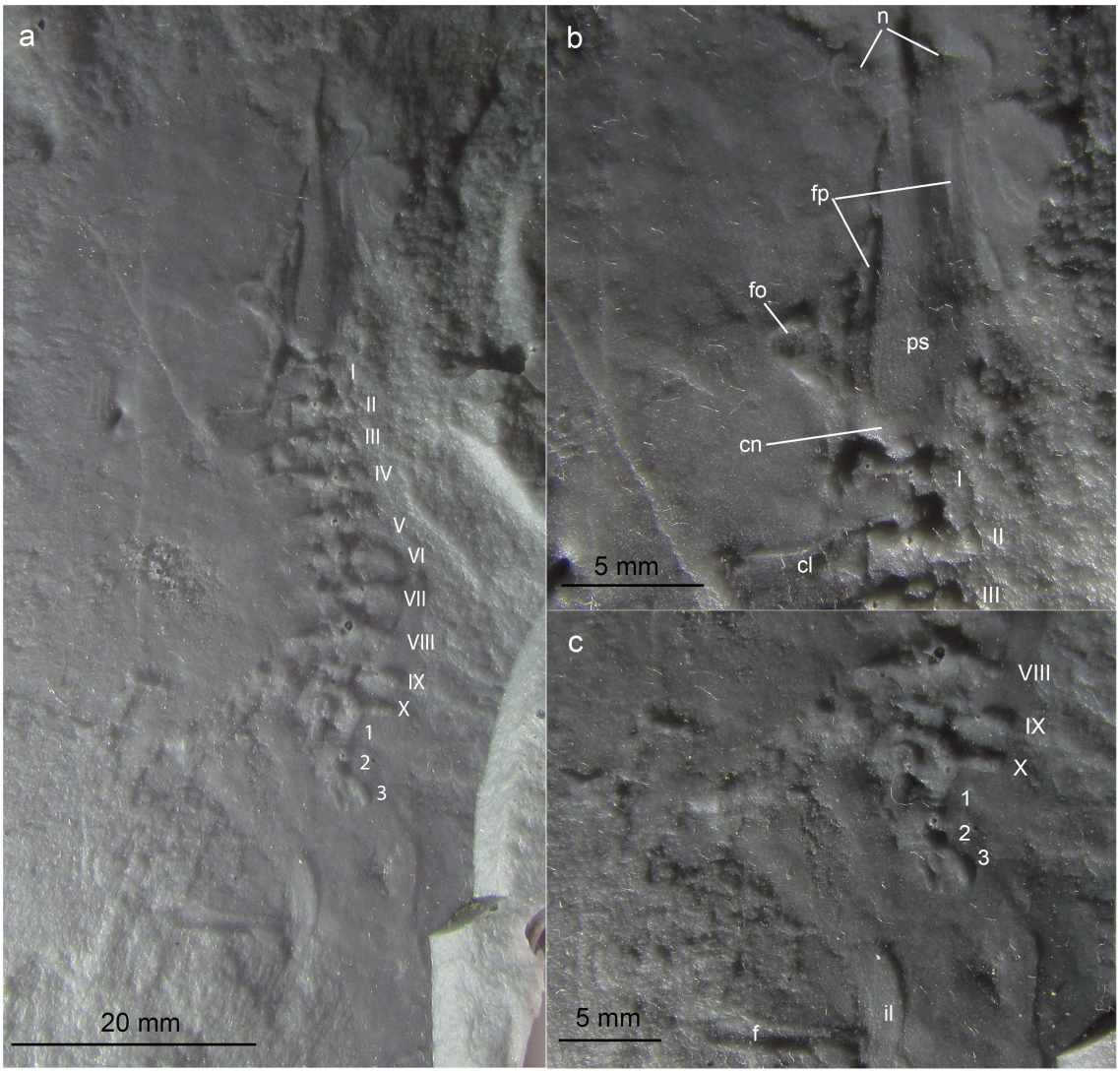

Extended Data Fig. 4 | Photographs of the latex cast of MPM-PV 23540 taken under low-angle light. a, Cast of the complete specimen showing the preserved vertebral elements; **b**, close-up of the skull and first vertebrae; **c**, close-up of the last vertebrae and appendicular elements. Abbreviations: cl, cleithrum; cn, chondrified neurocranium, f, femur; fo, fenestra ovalis; fp, frontoparietal; il, ilium; n, nasal; ps, parasphenoid; I–IX, presacral vertebrae; X, sacrum; 1–3 postsacral neural arches.

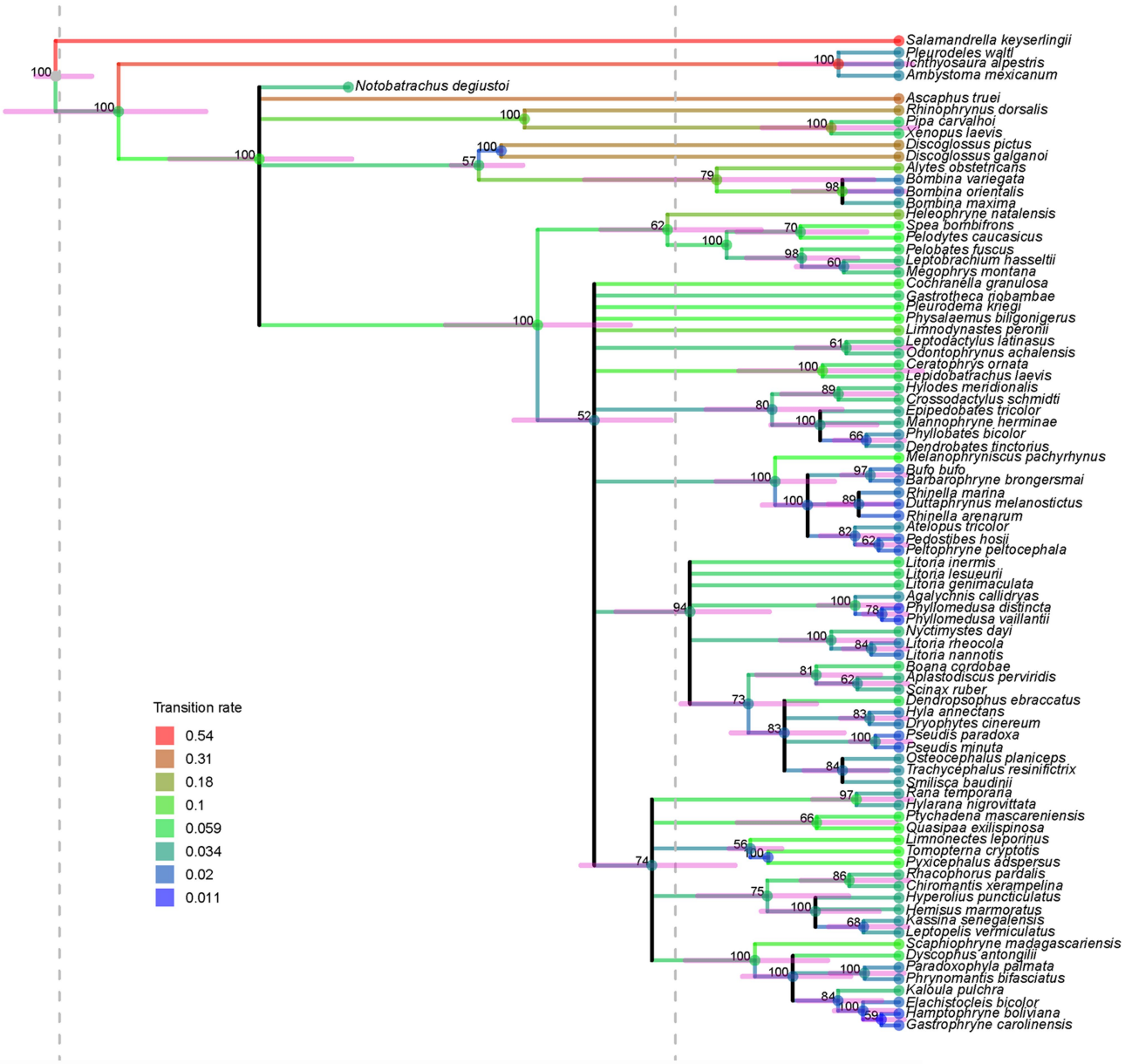

Extended Data Fig. 5 | Majority rule consensus tree recovered from the unconstrained Bayesian phylogenetic analysis depicting the position of the *Notobatrachus degiustoi* tadpole. Numbers at nodes indicate posterior probabilities and dotted grey vertical lines indicate the boundaries between the Permian and Triassic and Cretaceous and Palaeogene geological periods, respectively.

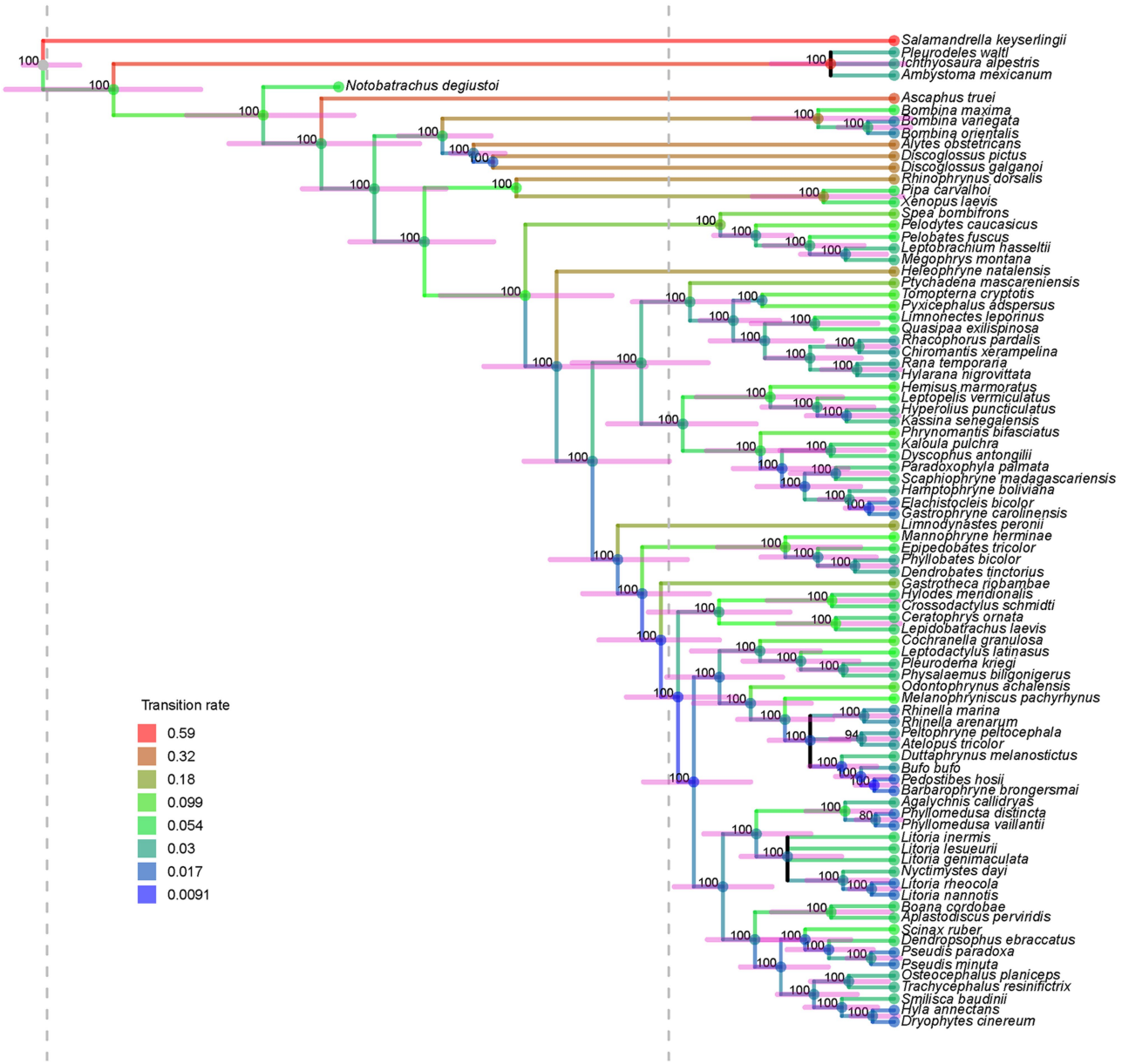

Extended Data Fig. 6 | Majority rule consensus tree recovered from the constrained Bayesian phylogenetic analysis using a molecular backbone, depicting the position of the *Notobatrachus degiustoi* tadpole. Numbers at nodes indicate posterior probabilities and dotted grey vertical lines indicate the boundaries between the Permian and Triassic and Cretaceous and Palaeogene geological periods, respectively.

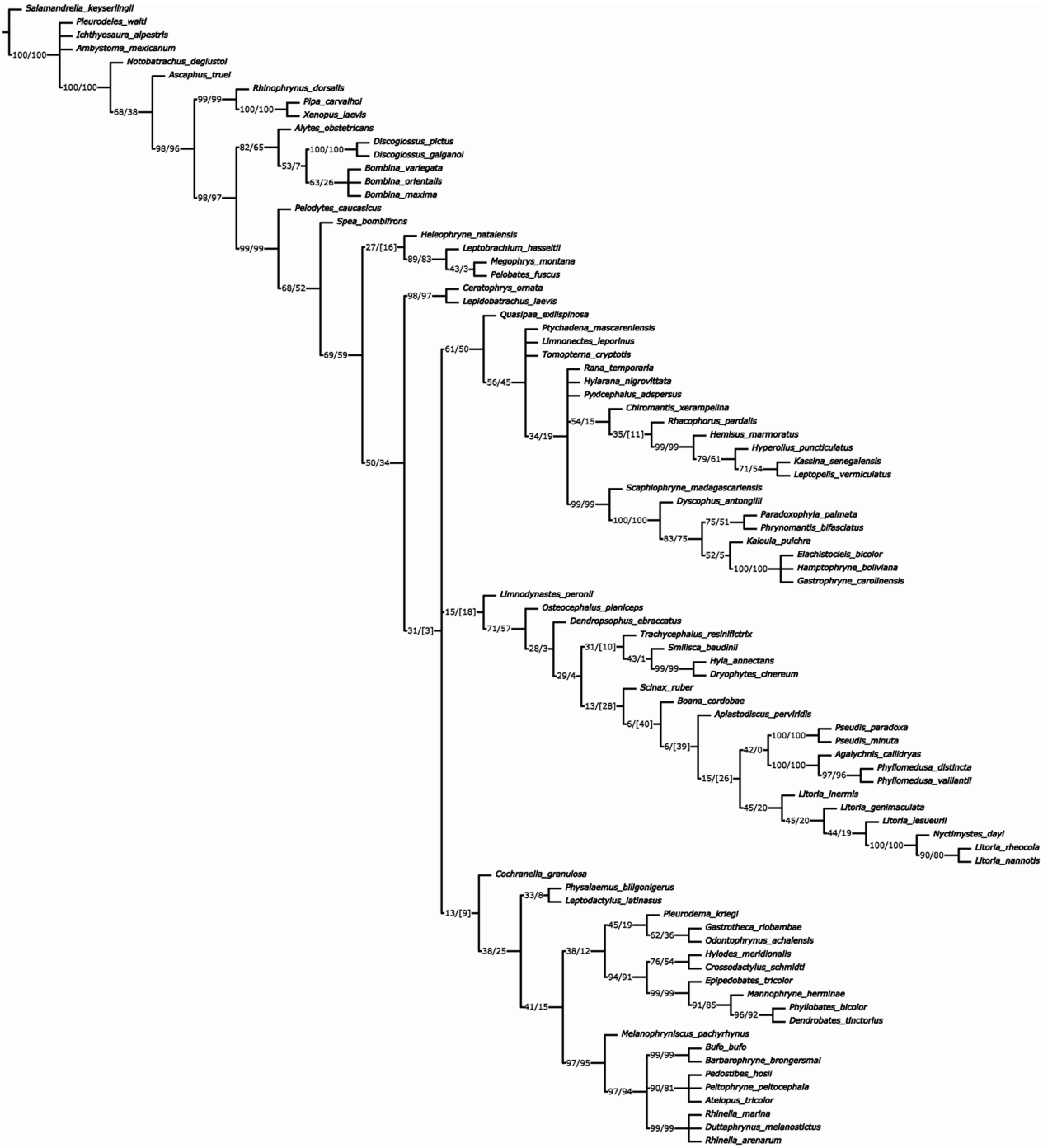

Extended Data Fig. 7 | Global strict consensus tree recovered from the unconstrained parsimony phylogenetic analysis depicting the position of the *Notobatrachus degiustoi* tadpole. Numbers above branches indicate absolute (left) and GC (group present/contradicted) (right) no-zero weight symmetric resampling frequencies (values between squared brackets are negative).

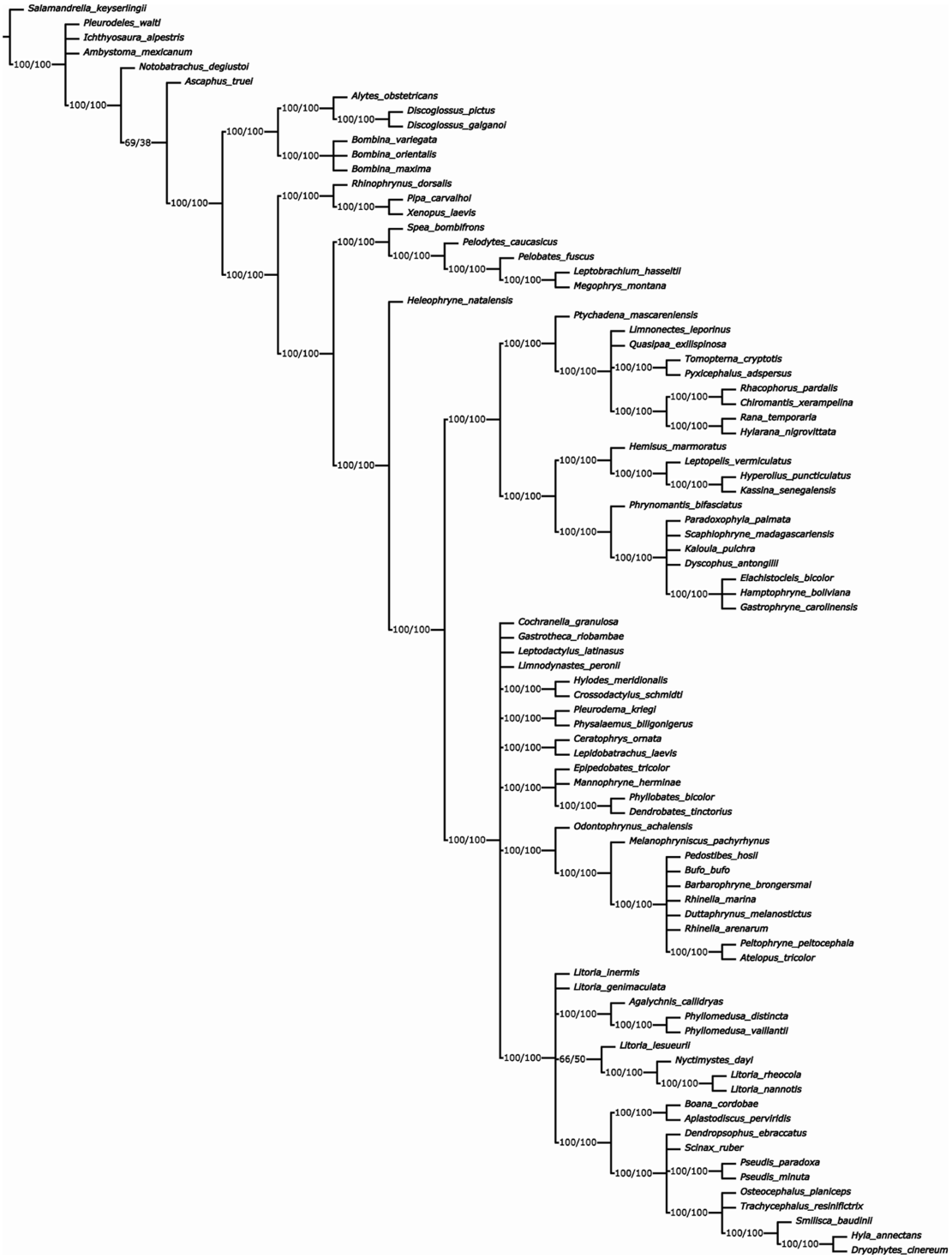

Extended Data Fig. 8 | Global strict consensus tree recovered from the constrained parsimony phylogenetic analysis using a molecular backbone, depicting the position of the *Notobatrachus degiustoi* tadpole. Numbers above branches indicate absolute (left) and GC (group present/contradicted) (right) no-zero weight symmetric resampling frequencies.

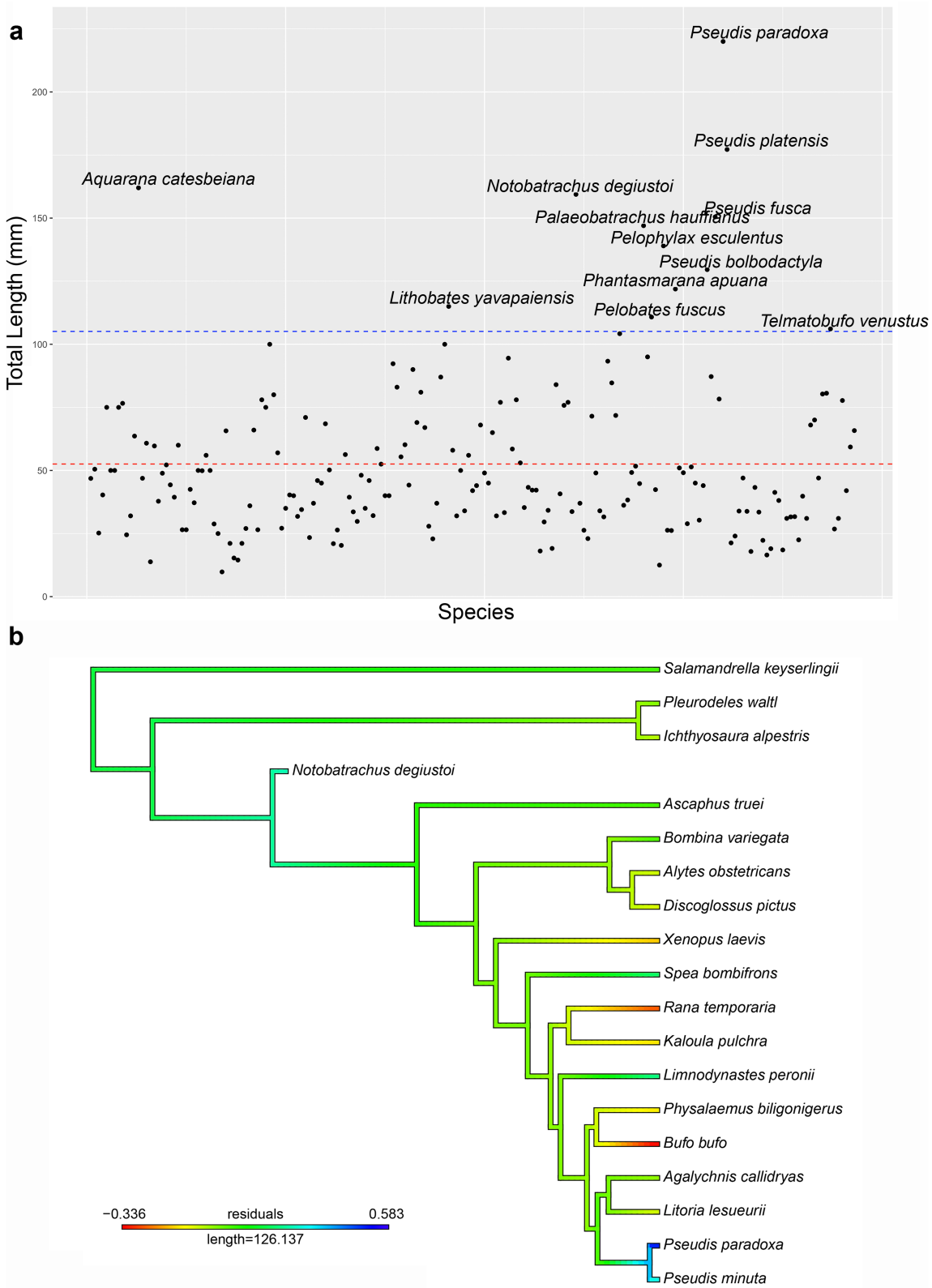

Extended Data Fig. 9 | Gigantism in anurans. a, Plot depicting the total length of tadpoles across 187 species with the inclusion of the *Notobatrachus degiustoi* tadpole. The red line denotes the mean of the surveyed values (50.94 mm), whereas the blue line denotes twice the mean (101.8 mm). Labelled species are those with gigantic tadpoles. **b**, Optimization of the residuals of the linear regression between the tadpole total length and adult snout-vent length in the Bayesian tip-dating tree (using mean ages), showing the independent acquisition of gigantism in *Notobatrachus degiustoi* and some crown-anuran species.

nature portfolio

Corresponding author(s): Mariana Chuliver

Last updated by author(s): Jul 25, 2024

Reporting Summary

Nature Portfolio wishes to improve the reproducibility of the work that we publish. This form provides structure for consistency and transparency in reporting. For further information on Nature Portfolio policies, see our Editorial Policies and the Editorial Policy Checklist.

Statistics

For all statistical analyses, confirm that the following items are present in the figure legend, table legend, main text, or Methods section.

n/a	Confirmed
☐	☒ The exact sample size (*n*) for each experimental group/condition, given as a discrete number and unit of measurement
☐	☒ A statement on whether measurements were taken from distinct samples or whether the same sample was measured repeatedly
☐	☒ The statistical test(s) used AND whether they are one- or two-sided *Only common tests should be described solely by name; describe more complex techniques in the Methods section.*
☒	☐ A description of all covariates tested
☐	☒ A description of any assumptions or corrections, such as tests of normality and adjustment for multiple comparisons
☐	☒ A full description of the statistical parameters including central tendency (e.g. means) or other basic estimates (e.g. regression coefficient) AND variation (e.g. standard deviation) or associated estimates of uncertainty (e.g. confidence intervals)
☐	☒ For null hypothesis testing, the test statistic (e.g. *F*, *t*, *r*) with confidence intervals, effect sizes, degrees of freedom and *P* value noted *Give P values as exact values whenever suitable.*
☐	☒ For Bayesian analysis, information on the choice of priors and Markov chain Monte Carlo settings
☒	☐ For hierarchical and complex designs, identification of the appropriate level for tests and full reporting of outcomes
☒	☐ Estimates of effect sizes (e.g. Cohen's *d*, Pearson's *r*), indicating how they were calculated

Our web collection on statistics for biologists contains articles on many of the points above.

Software and code

Policy information about availability of computer code

Data collection	No software was used for data collection.
Data analysis	TNT version 1.6; MrBayes 3.2.7; Tracer 1.7.1; and the R packages Claddis version 0.6.3, akima 0.6-3.4, and phytools 2.1-1. The custom code used for the disparity analysis is deposited in Figshare: https://figshare.com/s/4fc207d07da2b8ff13cd

For manuscripts utilizing custom algorithms or software that are central to the research but not yet described in published literature, software must be made available to editors and reviewers. We strongly encourage code deposition in a community repository (e.g. GitHub). See the Nature Portfolio guidelines for submitting code & software for further information.

Data

Policy information about availability of data

All manuscripts must include a data availability statement. This statement should provide the following information, where applicable:

- Accession codes, unique identifiers, or web links for publicly available datasets
- A description of any restrictions on data availability
- For clinical datasets or third party data, please ensure that the statement adheres to our policy

All data generated or analysed during the study are included as part of this article, and its supplementary information files. The datasets for phylogenetic, disparity and morphometric analyses are deposited in the Figshare repository (https://figshare.com/s/4fc207d07da2b8ff13cd).

Research involving human participants, their data, or biological material

Policy information about studies with human participants or human data. See also policy information about sex, gender (identity/presentation), and sexual orientation and race, ethnicity and racism.

Reporting on sex and gender	N/A
Reporting on race, ethnicity, or other socially relevant groupings	N/A
Population characteristics	N/A
Recruitment	N/A
Ethics oversight	N/A

Note that full information on the approval of the study protocol must also be provided in the manuscript.

Field-specific reporting

Please select the one below that is the best fit for your research. If you are not sure, read the appropriate sections before making your selection.

☒ Life sciences ☐ Behavioural & social sciences ☐ Ecological, evolutionary & environmental sciences

For a reference copy of the document with all sections, see nature.com/documents/nr-reporting-summary-flat.pdf

Life sciences study design

All studies must disclose on these points even when the disclosure is negative.

Sample size	No statistical methods were used to determine sample size. Terminals of the phylogenetic data matrices were scored based on all available, unambiguously referred specimens. Sample size was limited to available published information on phylogenetic analyses or published data on measurements of tadpoles and adult anurans.
Data exclusions	No exclusions were performed because taxonomic and character samples of the phylogenetic analyses were intended to be as broad as possible.
Replication	Our investigation considers all the available specimen of the studied species and the phylogenetic analyses include 86 taxa and 152 characters. Terminals of the phylogenetic data matrices were scored based on the type specimens and all available, unambiguously referred specimens. The parsimony phylogenetic analysis was conducted until 100 optimal results were recovered under the tree search replications. In the morphological disparity analyses, the 95% confidence intervals were generated using the two tails of values recovered from 9,999 bootstrap technical replicates. All the replications were successful.
Randomization	Not applicable. The available fossil material was included and the random and incomplete nature of the vertebrate fossil record acts as a natural randomization process.
Blinding	The taxon-character matrices for the phylogenetic analyses were built on the basis of independent observation of each taxon. Blinding was not necessary, neither possible, because we have used all available specimens for the scoring of characters in each sampled species.

Reporting for specific materials, systems and methods

We require information from authors about some types of materials, experimental systems and methods used in many studies. Here, indicate whether each material, system or method listed is relevant to your study. If you are not sure if a list item applies to your research, read the appropriate section before selecting a response.

Materials & experimental systems

n/a	Involved in the study
☒	☐ Antibodies
☒	☐ Eukaryotic cell lines
☐	☒ Palaeontology and archaeology
☒	☐ Animals and other organisms
☒	☐ Clinical data
☒	☐ Dual use research of concern
☒	☐ Plants

Methods

n/a	Involved in the study
☒	☐ ChIP-seq
☒	☐ Flow cytometry
☒	☐ MRI-based neuroimaging

Palaeontology and Archaeology

Specimen provenance	The specimen described (MPM-PV 23540) was collected from a quarry from the Middle Jurassic La Matilde Formation (Bathonian-Callovian; ca. 168–161 Mya) in southern Patagonia, Argentina. The fieldwork and curation was performed by authors of the manuscript following the national legislation.
Specimen deposition	MPM-PV 23540 is cataloged and available for study to researchers upon request at Museo Provincial Padre M.J. Molina, Santa Cruz Province, Argentina.
Dating methods	No new dating methods were performed. Dates used for the Bayesian inference analysis are provided in the supplementary information.

☒ Tick this box to confirm that the raw and calibrated dates are available in the paper or in Supplementary Information.

Ethics oversight	No ethical approval or guidance was required because the study is based on previously collected fossil specimens.

Note that full information on the approval of the study protocol must also be provided in the manuscript.

Plants

Seed stocks	N/A
Novel plant genotypes	N/A
Authentication	N/A